

**LARGE-SCALE VARIATIONS IN OZONE FROM THE FIRST  
TWO YEARS OF UARS MLS DATA**

*Lee S. Elson, Gloria Manney, Lucien Froidevaux, Joe W. Waters*

M/S 183-701  
Jet Propulsion Laboratory  
California Institute of Technology  
Pasadena, CA. 91109

March 15, 1994

ABSTRACT

Two years of stratospheric measurements of ozone from the Upper Atmosphere Research Satellite Microwave Limb Sounder are examined in order to characterize large horizontal scale wave variations. The use of **Fourier analysis** allows the detection of variations from daily through seasonal and interannual time scales. High latitude winter variations at 10 hPa often have very large amplitudes but smaller midlatitude variations are more ubiquitous. Some variations have the characteristics of **locally generated instabilities**. Correlations of wave features with changes in the zonal mean ozone at 10 hPa suggest significant wave/zonal mean interactions during strong **wintertime polar warming** events. Such correlations are not evident at other levels. Spectral analysis of the large-scale variations show most waves to be slowly propagating. In contrast to some past observations, equatorial regions are shown to lack large amplitude wave events.

## 1. Introduction

Planetary scale waves are known to be important mechanisms for transport processes in the middle atmosphere. There are many indicators of wave activity including temperature and species concentrations. Each of these indicators has been studied in the past for insight into a variety of wave mechanisms. This discussion will focus on an overview of wave variations in ozone concentration as measured during the first two years of operation of the Microwave Limb Sounder (MLS) [Barath et al., 1993], on the Upper Atmosphere Research Satellite (UARS) [Reber, 1990]. A companion paper (Froidevaux et al., 1994) traces the evolution of zonal mean ozone over a similar period.

There are several reasons why the MLS data set provides a unique view of ozone in the middle atmosphere. Its vertical resolution (about 4 km) is superior to the Total Ozone Mapping Spectrometer (TOMS) and Nimbus-7 Solar Backscatter Ultraviolet (SBUV) measurements. In addition, unlike SBUV and TOMS, MLS is able to detect ozone during the night. The Limb Infrared Monitor of the Stratosphere (LIMS) on Nimbus-7 had capabilities similar to MLS, but only provided data for about 8 months, whereas MLS is well into its third year of operation and is thus able to provide information on seasonal and interannual variations. In addition, LIMS was unable to view latitudes south of about  $-64^{\circ}$ . Although MLS is able to view latitudes as far south as  $-80^{\circ}$ , it cannot do so all of the time. Because UARS performs a yaw maneuver approximately every 36 days (one UARS "month"), MLS alternately views latitudes from about  $-34^{\circ}$  to  $80^{\circ}$  and from  $34^{\circ}$  to  $-80^{\circ}$ . Although the mid and high latitudes are undersampled by this viewing procedure, the low latitudes ( $\pm 34^{\circ}$ ) are sampled continuously, except for data outages.

One area of focus in past studies has been that of ozone variability on seasonal to interannual time scales. Perliski and London (1989) examined 9 years of SBUV data. Among their findings were that longitudinal wavenumber 1 variations had largest amplitudes in the polar regions with a secondary maximum over the equator. The Northern

Hemisphere maximum appeared to be larger than that of the Southern Hemisphere. Randel (1993) also analyzed SBUV data and found evidence that planetary wave events associated with polar warmings can influence zonal mean ozone over nearly the entire globe. It must be noted, however, that according to Randel and Gille (1991) SBUV data may underestimate wave amplitudes by 20%-60% depending on the vertical structure of the disturbance.

Planetary scale waves have been examined on shorter time scales as well. Kelvin waves hold a great deal of interest because they serve to transport momentum and chemical species in the tropics. Salby et al. (1990) and Randel (1990) examined ozone power spectra from LIMS observations and found a clear Kelvin wave signature (eastward propagating wave 1 and 2 variations with periods ranging from about 4 to 40 days). Canziani et al. (1994) provide a similar study using MLS data. Their discussion of ozone variations associated with Kelvin waves focuses on two time periods near the solstices during the first UARS year. They found similarities with the earlier LIMS studies but also some differences including a greater amount of asymmetry about the equator. Kelvin wave amplitudes in ozone concentration are typically at least an order of magnitude smaller than other variations and are therefore not evident in the figures discussed here.

LIMS observations have also been used to investigate another important source of planetary waves: instability. It is well known that unstable disturbances are generated near the equatorial and polar flanks of the polar night wind jet. For example, Elson (1990) found that during the winter months in 1979, an unstable mode centered near  $20^{\circ}$  and 10 hPa was evident in the ozone field. The small vertical scale (about 10 km) of this type feature would make it hard to properly measure in SBUV data. This instability traveled westward with a period near 13 days.

The purpose of the discussion here is to provide an overview of planetary scale ozone variations as measured by MLS from October 1991 through September of 1993. Section 2 will describe the method used to analyze the data. Section 3 will present an overview of

wave activity at several pressure levels for each of the 2 years. In addition, several limited time periods will be examined in greater detail. Comparisons will be made between the time evolution in the zonal mean and wavenumber 1 ozone. Section 3 will also examine the variance spectra for midlatitude disturbances and will provide examples of the vertical structure of these disturbances. Comparisons will be made with earlier studies.

## **2. Data analysis: Fourier transforms**

Elson and Froidevaux (1993), referred to here as EF, have described the production of synoptic MLS maps. The approach begins with a coordinate system rotation in order to calculate Fourier transforms of the time and longitude dependence of ozone concentration. This technique, described by Salby (1982a,b), makes use of fast Fourier transforms at selected latitudes and heights to produce Fourier transform coefficients for discrete values of  $m$ , the longitudinal wavenumber, and  $\sigma$ , the frequency. The input series must be equally spaced in longitude and time, a requirement made more difficult by the variability of the UARS orbital period. This variability is small enough to allow the routine calculation of Fourier coefficients over a 7.2 day (108 orbit) period and unless otherwise indicated, these coefficients are used here. Longer calculations (e.g. over a UARS month) are possible only during times when the orbital period is very slowly changing. As discussed by Elson (1990), there is a tradeoff between better frequency resolution and interference caused by transience as one increases the sample length. The 60 day sample lengths, found useful for analyzing LIMS data, are not possible using the present approach unless a re-mapping [e.g. Canziani et al. (1994)] is carried out. Nevertheless the frequency resolution obtained here with sample lengths of order 30 days is quite adequate.

Once the Fourier transform coefficients have been determined, the sine and cosine components are used to calculate the cross-spectral and power spectral density functions,

as described by Bendat and Piersol (1971). These functions are then spectrally smoothed using a Hanning window. This smoothing is necessary, in part, in order to provide reasonable estimates of statistical significance. Such estimates are found by calculating coherency and relating it to a posteriori probability by the relation

$$\beta = 1 - [1 - p]^{-1 + \frac{df}{2}}, \quad (1)$$

where  $\beta$ ,  $p$  and  $df$  are the coherency, probability and degrees of freedom respectively.  $df=6$  for the Hanning window used here. The spectral density functions are also used to find the eastward and westward propagating wave variances described by Schäfer (1979). As discussed by EF, the Fourier series corresponding to the ascending and descending parts of the orbit cease to be independent as one approaches the turning points of the orbit. This can produce artifacts in the form of scalloping effects poleward of  $\pm 75^\circ$ .

In addition to producing a synoptic map, (i.e. concentration at one time and altitude but all latitudes and longitudes) the above procedure makes it possible to examine the time evolution of various longitudinal components of the ozone field. This is accomplished by evaluating the inverse Fourier transform at one day intervals using only Fourier coefficients for the selected wavenumber. Missing days (e.g. UARS yaw maneuvers, field-of-view contamination from the moon, platform and instrument problems) are simply omitted, resulting in gaps.

### 3. Results

#### a. Time evolution of wavenumber components

The zonally averaged ( $m=0$ ) component of ozone concentration during the first two years of observations shows several interesting features, as discussed by Froidevaux et al. (1994). The absolute value of the  $m=1$  component of wave variance, at pressure levels of

46, 10 and 2 hPa (UARS levels 8,12 and 16) are shown here in Fig. 1. Wave activity is seen to be transient in nature but predominant during the fall, winter and spring months in each hemisphere and at all levels shown. Of the three levels, 10 hPa exhibits the largest amplitude. Interannual variability can also be seen at all levels, with a very large difference occurring near  $60^\circ$  at 10 hPa during December and January (UARS days 84-124 and 446-485). Note that UARS began its operation on September 12, 1991 (UARS day 1).

The results for  $m=2$  are similar in structure to those for  $m=1$  but the amplitudes are generally smaller. Figure 2 shows these amplitudes at the same levels as Fig. 1. Although both wave 1 and wave 2 are usually present during the active months, there are some noteworthy departures from this pattern. Days 54-83 (November 1991) show the southern midlatitudes to be quite active with wave 2 events, but nearly devoid of wave 1 at 10 hPa. Similarly, days 626-665 (June 1993) contain significant levels of wave 1 activity but little wave 2 in this same latitude region at 46 hPa. Manney et al. (1991) found similar behavior when they examined the height field from National Meteorological Center (NMC) data.

Closer inspection of Fig. 1 yields several interesting features. Wave activity appears to be strongest, especially at 10 hPa, in two somewhat distinct bands: one between  $60 - 80^\circ$  and a second, smaller one in the  $20 - 35^\circ$  range. The equatorial region seems particularly devoid of large amplitudes. These results are in marked contrast to the SBUV results of Perliski and London (1989) described above, but are quite similar to the LIMS results described by Elson (1990).

Figures 1 and 2 lead to the question of whether the time and latitude structure of the wave events can be linked to a mechanism. As discussed above, one possibility is locally generated instabilities. The latitude gradient of potential vorticity (PV) can provide an indicator of the likelihood of instability, at least in the small amplitude approximation (Manney et al., 1988). Figure 3 shows this quantity on the 840 K potential temperature surface (near 10 hPa), derived from UK Meteorological Office data using the technique

described by Manney and Zurek (1993), for the two years shown in Figs. 1 and 2. The white contours show zero values of the PV gradient, i.e. the region where the necessary condition for instability is satisfied. The temporal correlation with large wave events at high latitudes in both hemispheres is stronger during the spring months. This is consistent, at least in the Southern Hemisphere, with past suggestions (Manney et al., 1991b) that instability in the polar regions is most important during the spring breakup of the vortex. According to the results of Manney et al., (1991a) there is considerable interannual variability in the location and timing of sign changes in PV. This is reflected in Fig. 3 where the area bounded by white contours in October is much greater in 1992 than 1991. In Fig. 4, we focus on a late winter period (days 518-554) in the Northern Hemisphere. This figure shows the PV gradient and the wave 2 variance amplitude. The most extensive region bounded by zero gradient values corresponds in time and latitude to the largest  $m=2$  amplitude poleward of  $60^\circ$  between days 541 and 550. Although this structure is similar to that found by Manney et al. (1991a) for height fields in the Southern Hemisphere, a more definitive identification of mechanisms requires an examination of the height and temperature fields for this time period. As discussed by Elson (1990) the spatial structure of unstable disturbances in ozone and temperature can be quite different.

By expanding the time axes in Fig. 1 and comparing  $m=0$  and  $m=1$  amplitudes, one can see a significant variation with altitude in how the waves and the zonal mean interact. Several periods with large wave amplitudes have been selected for discussion. Fig 5a and b show the  $m=0$  and  $m=1$  variance amplitude components for February and March of 1993 at 2 hPa. At these levels, there does not seem to be much temporal correlation between changes in zonal mean ozone and wave 1 amplitude. This behavior is typical for the 2 hPa data examined here and is in disagreement with the findings of Randel (1993) based on SBUV data from 1979-1981.

At 10 hPa in August and September of 1992, (Fig. 5c and d) the situation is quite different. Here we see that not only are the wave 1 amplitudes larger, there is a definite

signature in the zonal mean which corresponds in time and latitude to the large amplitude, transient wave events near days 361 and 371. These warming events were described by Fishbein et al. (1993) who noted their approximate 9 day periodicity. The time evolution of the zonal mean concentration implies that there is at least temporary poleward transport of ozone during the buildup of the wave 1 event. This type of correlation is not uncommon at 10 hPa and always has similar characteristics.

At 46 hPa, during the northern winter of 1991, large wave 1 amplitudes appear in the same latitude band as the large time tendencies in the zonal mean, as shown in Fig 5e and f. The time correlation between the two, however, is not obvious. As is the case at 2 hPa, the mean ozone concentration near 60° shows evidence of changes by the creation or deletion of closed contours, as would be the result of vertical transport. This is in contrast to the behavior at 10 hPa (Fig. 5c) where mean changes result from bending of existing contours as would be the case with horizontal transport. Much of the structure at 46 hPa is likely to be determined by the position and dynamics of the polar vortex.

#### b. Spectral analysis and spatial structure of selected features

The wave 1 and 2 ozone variations described above have distinctive vertical structure as well as preferred frequencies. Fishbein et al. (1993) characterized warming events during an active period in the Southern Hemisphere. Here, we describe a more quiescent period, when MLS was looking south. For the period chosen, Jan. 10- Feb. 8, 1993 (UARS days 487-516) the UARS orbital period was quite constant, allowing a 30 day record to be used for spectral analysis. The amplitude of the wave 1 and 2 variance is shown, at several altitudes, in Fig. 6 as a function of latitude and frequency. Several panels in this figure show large amplitudes near the 1 day westward propagating limit of the diagram. These large amplitudes are the result of a small systematic difference in the ascending and descending branches of the MLS data and should be regarded as artificial.

Some panels also show significant amplitude very near the polar limit of the data. As discussed above, this is the result of the lack of independence between the ascending and descending data sets in this region. From Fig. 6, it can be seen that there is significant variation of both the latitude structure and propagation characteristics with altitude. In general, the spectra are peaked at the smaller frequencies (usually referred to as "red") but much of the slow moving variance changes from eastward to westward and back to eastward as one moves from 2 to 10 to 22 hPa. In addition, there is a relative maximum centered at the equator at 2 and 22 hPa, but not at 10 hPa. The largest amplitudes occur at 10 hPa and  $+25^\circ$  and at 22 hPa and  $-65^\circ$ . Wave 2 also has its largest amplitude in this latter region.

We can examine the latitude and height structure of variance amplitude in a frequency band where that variance is large. Figure 7 shows the height/latitude structure of the variance amplitude in a band centered at a period of 15 days (westward) for this same time in 1993. Two features are evident in both wave 1 and 2, one near  $+30^\circ$  and 10 hPa and one near  $-60^\circ$  and 20 hPa. Both features are of limited vertical extent with the more poleward feature showing a greater degree of coherency between the cosine and sine components. The midlatitude feature has structure quite similar to that observed in the LIMS data (see Fig. 7 of Elson, 1990).

#### 4. Discussion

Large scale wave variance in the ozone concentration measured by UARS MLS shows a strong dependence on season, latitude and altitude as well as interannual variation. As expected, amplitudes are largest in the winter polar regions. Variations frequently peak near 10 hPa and it is at this altitude that wave/zonal mean interactions are most obvious suggesting that horizontal transport is especially important, at least in the polar and

midlatitude regions. Many of the ozone disturbances detected by MLS are of very limited vertical extent so that differences with SBUV observations might be expected. For example, the characteristics of SBUV data which implied strong interactions between waves and the mean ozone concentrations, attributed to the 2 hPa level may have had a contribution from the lower altitudes.

It is more difficult to explain differences between SBUV and MLS observations of equatorial variations. The SBUV results for a 9 year average showed significantly more amplitude between  $\pm 20^\circ$  than for either of the MLS years. Whether this difference represents a real trend or an artifact in one or both data sets remains to be determined.

*Acknowledgements.* The authors thank the UARS project and the MLS team for providing support and the UKMO for supplying data. This research was sponsored by NASA's Upper Atmosphere Research Satellite Project and was performed at the Jet Propulsion Laboratory, California Institute of Technology under contract with the National Aeronautics and Space Administration.

REFERENCES

- Barath, F.T., M.C. Chavez, R.E. Cofield, D.A. Flower, M.A. Frerking, M.B. Gram, W.M. Harris, J.R. Holden, R.F. Jarnot, W.G. Kloezezan, G.J. Klose, G.K. Lau, M.S. Loo, B.J. Maddison, R.J. Mattauch, R.P. McKinney, G.E. Peckham, H.M. Pickett, G. Siebes, F.S. Soltis, R.A. Suttie, J.A. Tarsala, J.W. Waters, and W.J. Wilson, 1993: The Upper Atmosphere Research Satellite Microwave Limb Sounder Instrument. *J. Geophys. Res.*, **98**, 10,751-10,762.
- Canziani, P. O., J. R. Holton, E. Fishbein, L. Froidevaux and J. W. Waters, 1994: Equatorial Kelvin waves: A UARS-MLS view. *J. Atmos. Sci.*, this issue.
- Elson, L. S., 1990: Satellite observations of instability in the middle atmosphere. *J. Atmos. Sci.*, **47**, 1065-1074.
- and L. Froidevaux, 1993: The use of Fourier Transforms for asynoptic mapping: Applications to the Upper Atmosphere Research Satellite Microwave Limb Sounder. *J. Geophys. Res.*, **98**, 23039-23049.
- Fishbein, E. F., L. S. Elson, L. Froidevaux, G. L. Manney, W. G. Read, J. W. Waters, and R. W. Zurek, 1993: MLS observations of stratospheric waves in temperature and ozone during the 1992 southern winter. *Geophys. Res. Lett.*, **20**, 1255-1258.
- Froidevaux, L. et al., 1994: this issue.
- Manney, G. L., T. R. Nathan, and J. L. Stanford, 1988: Barotropic stability of realistic stratospheric jets. *J. Atmos. Sci.*, **45** 2545-2555.
- , C. R. Mechoso, L. S. Elson, and J. D. Farrara, 1991a: Planetary scale waves in the Southern Hemisphere winter and early spring stratosphere: Stability analysis. *J. Atmos. Sci.* **48**, 2509-2523.
- , J. D. Farrara, and C. R. Mechoso, 1991b: The behavior of wave 2 in the southern hemisphere stratosphere during late winter and early spring. *J. Atmos. Sci.*, **48**, 976-998.

- , and R. W. Zurek, 1993: Interhemispheric comparison of the development of the stratospheric polar vortex during fall: A 3-dimensional perspective for 1991-1992. *Geophys. Res. Lett.*, **20**, 1275-1278.
- Perliski, L. M. and J. London, 1989: Satellite observed long-term averaged seasonal and spatial ozone variations in the stratosphere. *Planet. Space Sci.*, **37**, 1509-1525.
- Randel, W. J., 1990: Kelvin wave-induced trace constituent oscillations in the equatorial stratosphere. *J. Geophys. Res.*, **95**, 18,641-18,652.
- , 1993: Global variations of zonal mean ozone during stratospheric warming events. *J. Atmos. Sci.*, **50**, 3308-3321.
- , and J. C. Gille, 1991: Kelvin wave variability in the upper stratosphere observed in SBUV ozone data. *J. Atmos. Sci.*, **48**, 2336-2349.
- Reber, C. A., 1990: The Upper Atmosphere Research Satellite. *EOS Trans. AGU*, **71**, 1867-1878.
- Salby, M. L., 1982a: Sampling theory for synoptic satellite observations. Part I: Space-time spectra, resolution and aliasing. *J. Atmos. Sci.*, **39**, 2577-2600.
- , 1982b: Sampling theory for synoptic satellite observations. Part II: Fast Fourier synoptic mapping. *J. Atmos. Sci.*, **39**, 2601-2614.
- , P. Callaghan, S. Solomon and R. R. Garcia, 1990: Chemical fluctuations associated with vertically propagating equatorial Kelvin waves. *J. Geophys. Res.*, **95**, 20,491-20,505.
- Schäfer, J., 1979: A space-time analysis of tropospheric planetary waves in the Northern Hemisphere. *J. Atmos. Sci.*, **36**, 1117-1123.

### Figure Captions

Figure 1. Time evolution of the amplitude of wave 1 ozone variance (ppmv) at a) 2 hPa for UARS days 20-375, b) 2 hPa for UARS days 380- 736, c) 10 hPa for UARS days 20-375, d) 10 hPa for UARS days 380-736, e) 46 hPa for UARS days 20-375, and f)46 hPa for UARS days 380-736.

Figure 2. Same as Fig. 1 but for wave 2 ozone variance.

Figure 3. Potential vorticity gradient ( $10^{-4} Km^2 kg^{-1} s^{-1} degree^{-1}$ ) on an 840 K potential temperature surface for a) the first UARS year (days 20-375) and b) the second UARS year (days 380-736). The zero value is highlighted by a white contour.

Figure 4. a) Wave 2 ozone variance amplitude (ppmv) versus time for UARS days 518-554 (Feb. 10, 1993 - Mar. 18, 1993) at 10 hPa and b) potential vorticity gradient on an 840 K potential temperature surface ( $10^{-4} Km^2 kg^{-1} s^{-1} degree^{-1}$ ) for the same period. The zero value is highlighted by a white contour.

Figure 5. Zonally averaged [a), c), e)] and wave 1 variance amplitude [b), d), f)] of ozone (ppmv) versus time at 2 hPa [a) and b)], 10 hPa [c) and d)] and 46 hPa [e) and f)]. a) and b) cover a period in Feb. and Mar. of 1993, c) and d) Aug. and Sep. of 1992 and e) and f) Dec. 1991 and Jan. 1992.

Figure 6. Wave variance amplitude of ozone (ppmv) at: a) 2 hPa, b) 10 hPa and c) 22 hPa. All panels are for wave 1 except d) which shows wave 2 at 22 hPa. UARS days 487-516 are covered. Color and contour scales are logarithmic.

Figure 7. a) Wave 1 variance amplitude of ozone (ppmv) versus altitude and latitude for variations with periods between 11.9 and 20.9 days. Shaded region denotes areas where the coherency corresponds to a probability of 90% or more. b) Same as a) but for wave 2. UARS days 487-516 are covered.

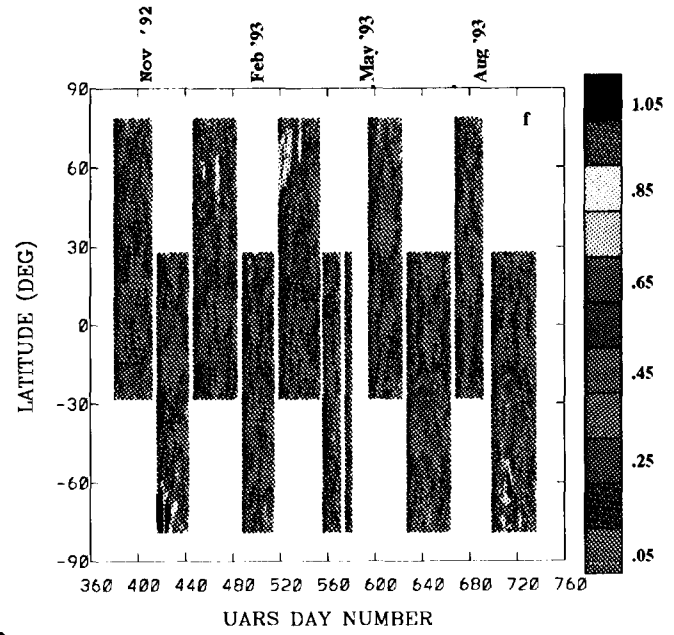
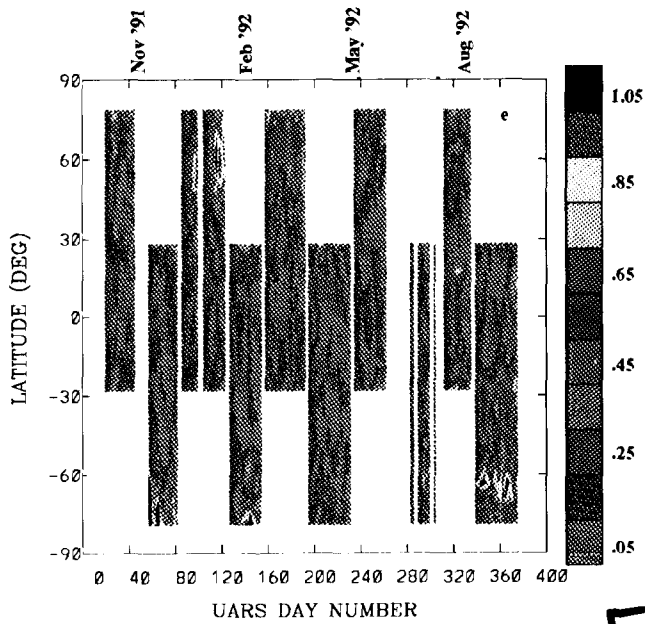
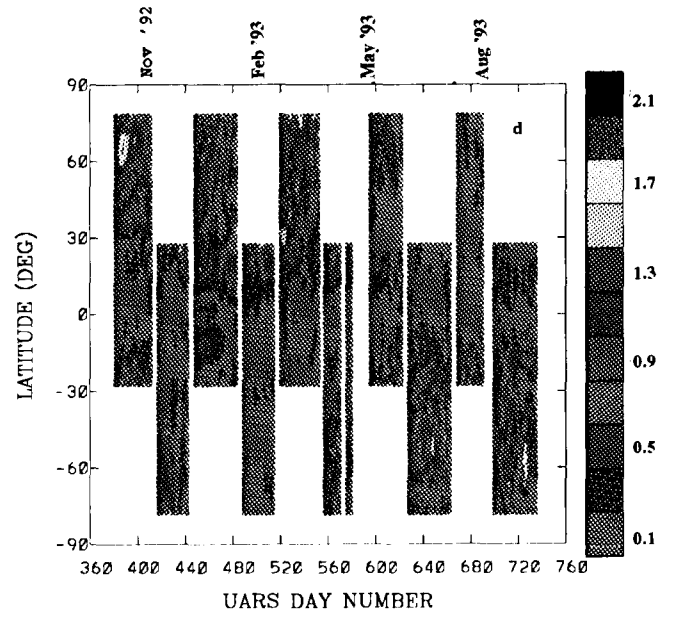
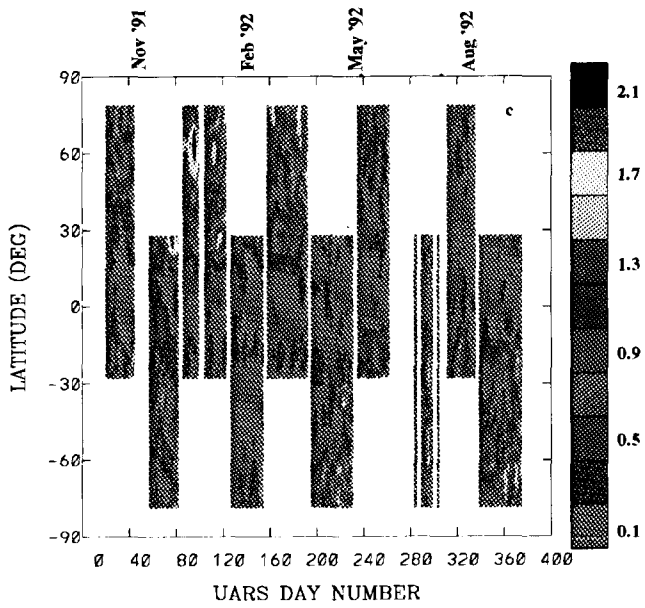
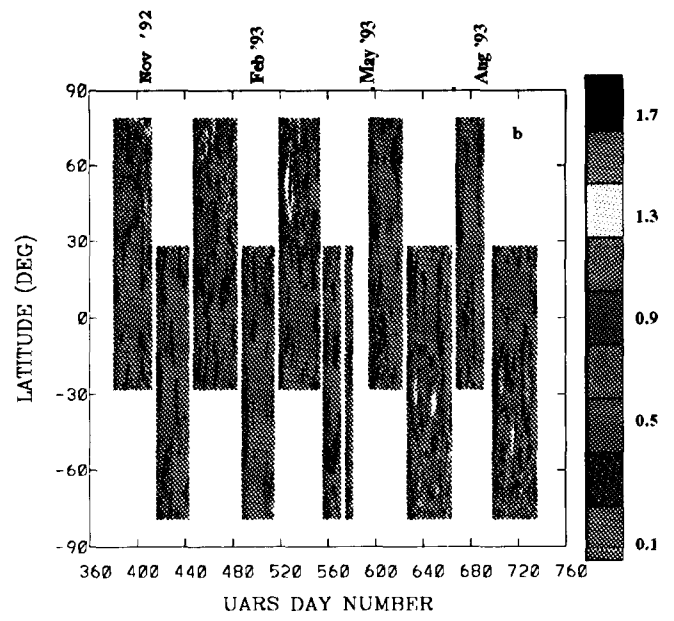
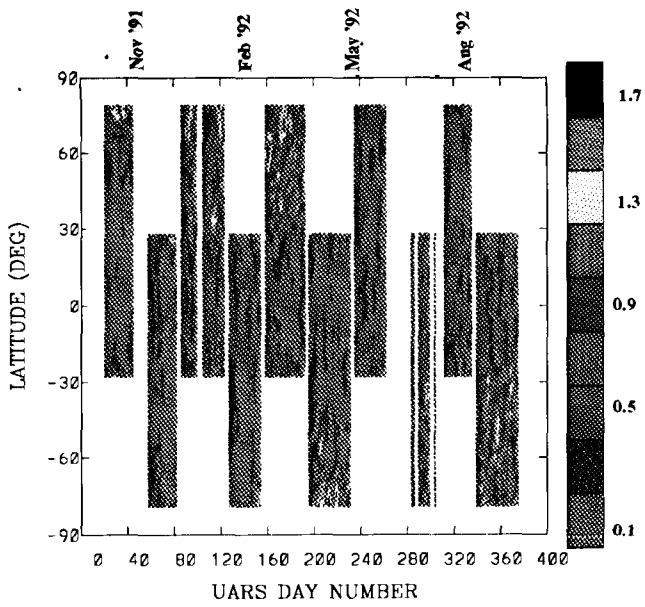


Fig 1

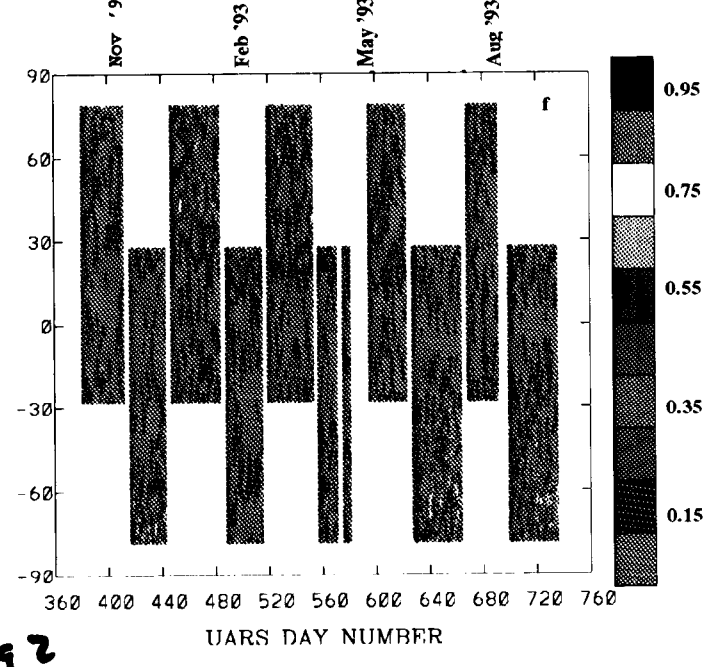
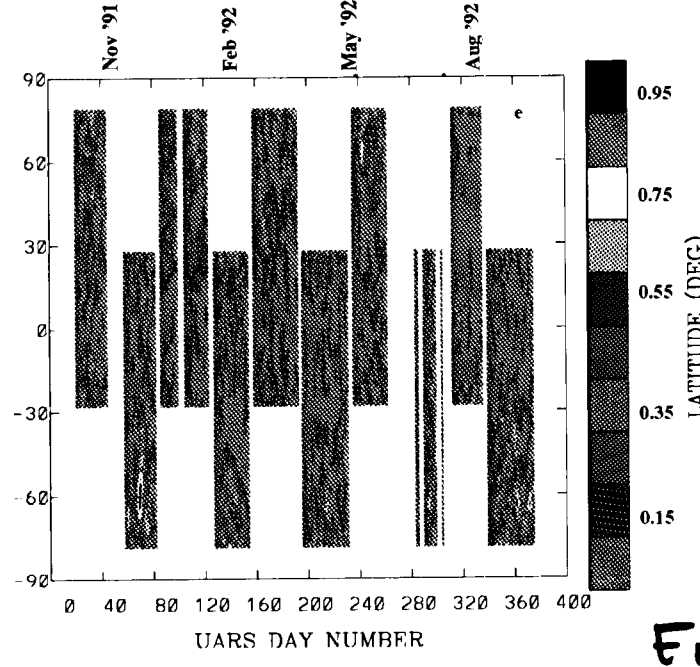
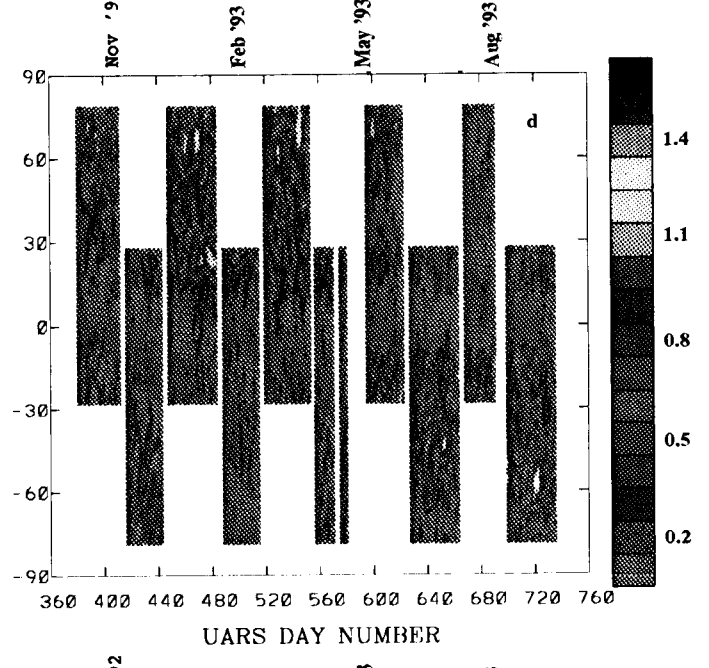
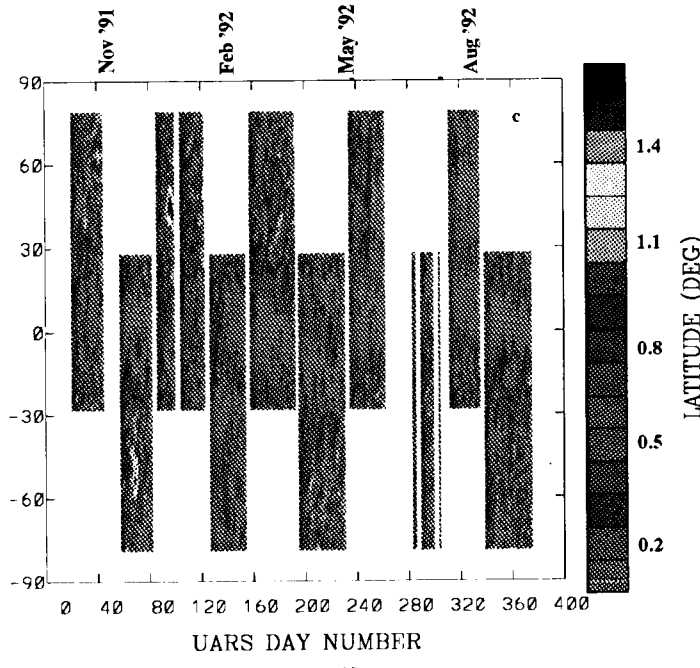
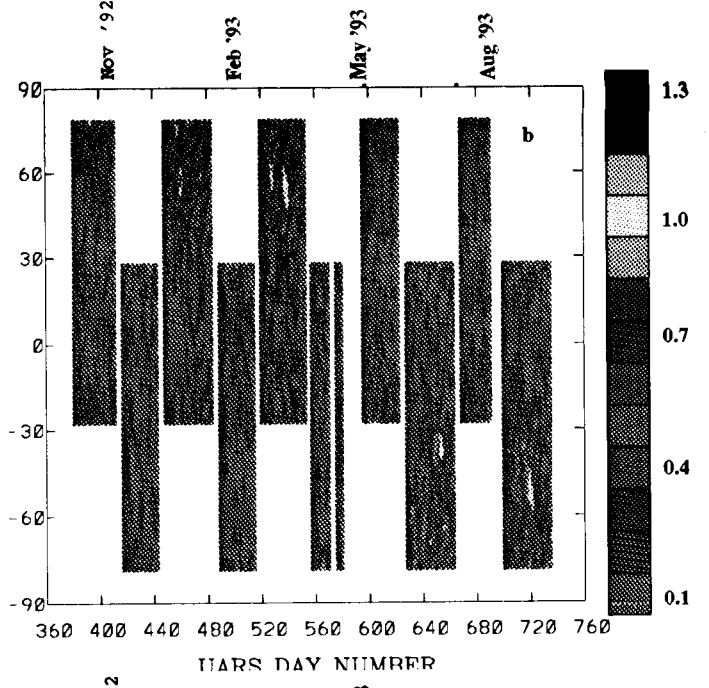
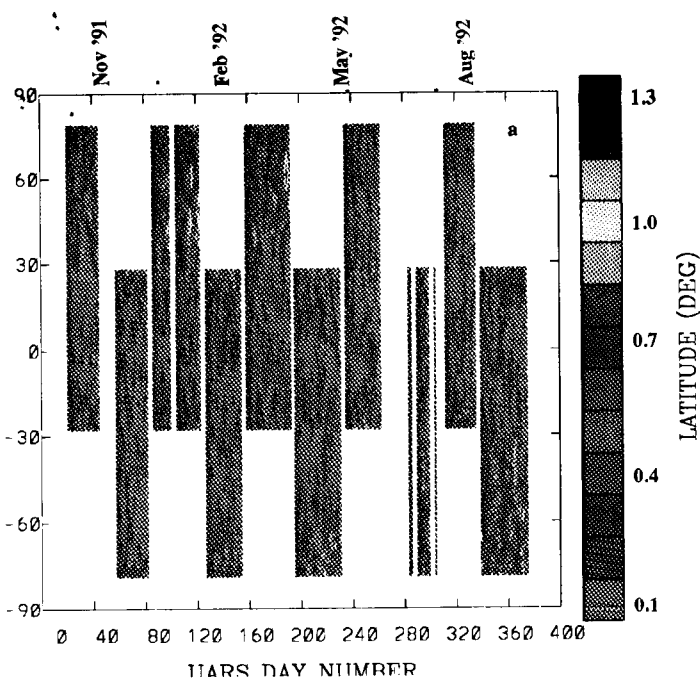


Fig 2

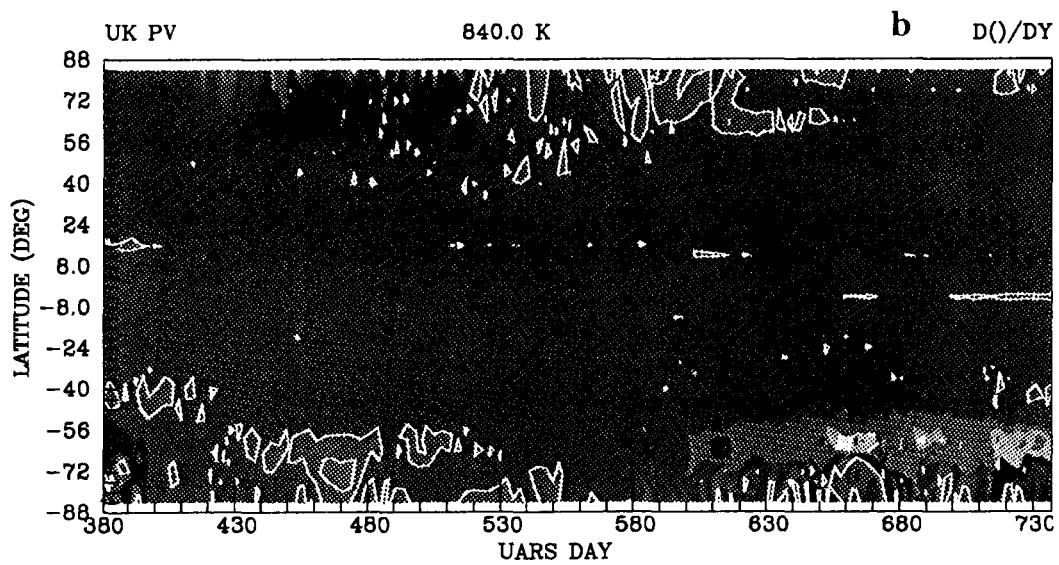
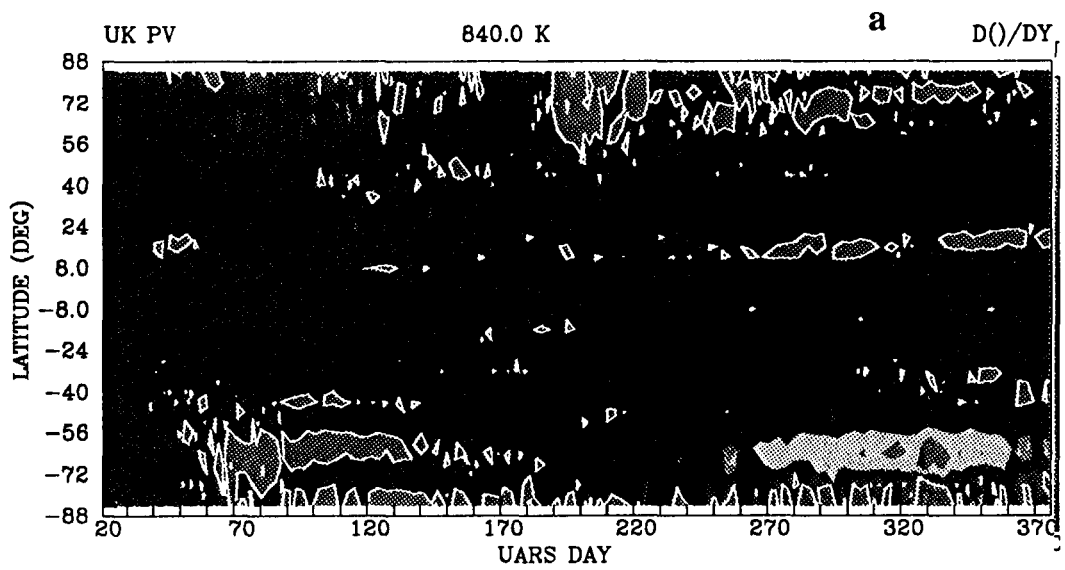


Fig 3

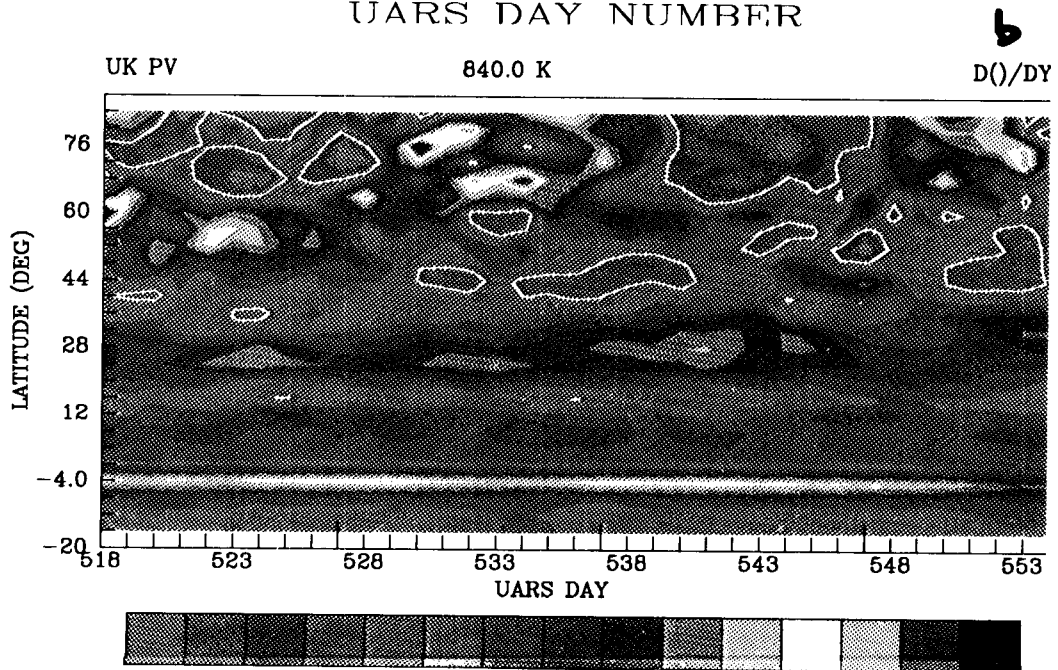
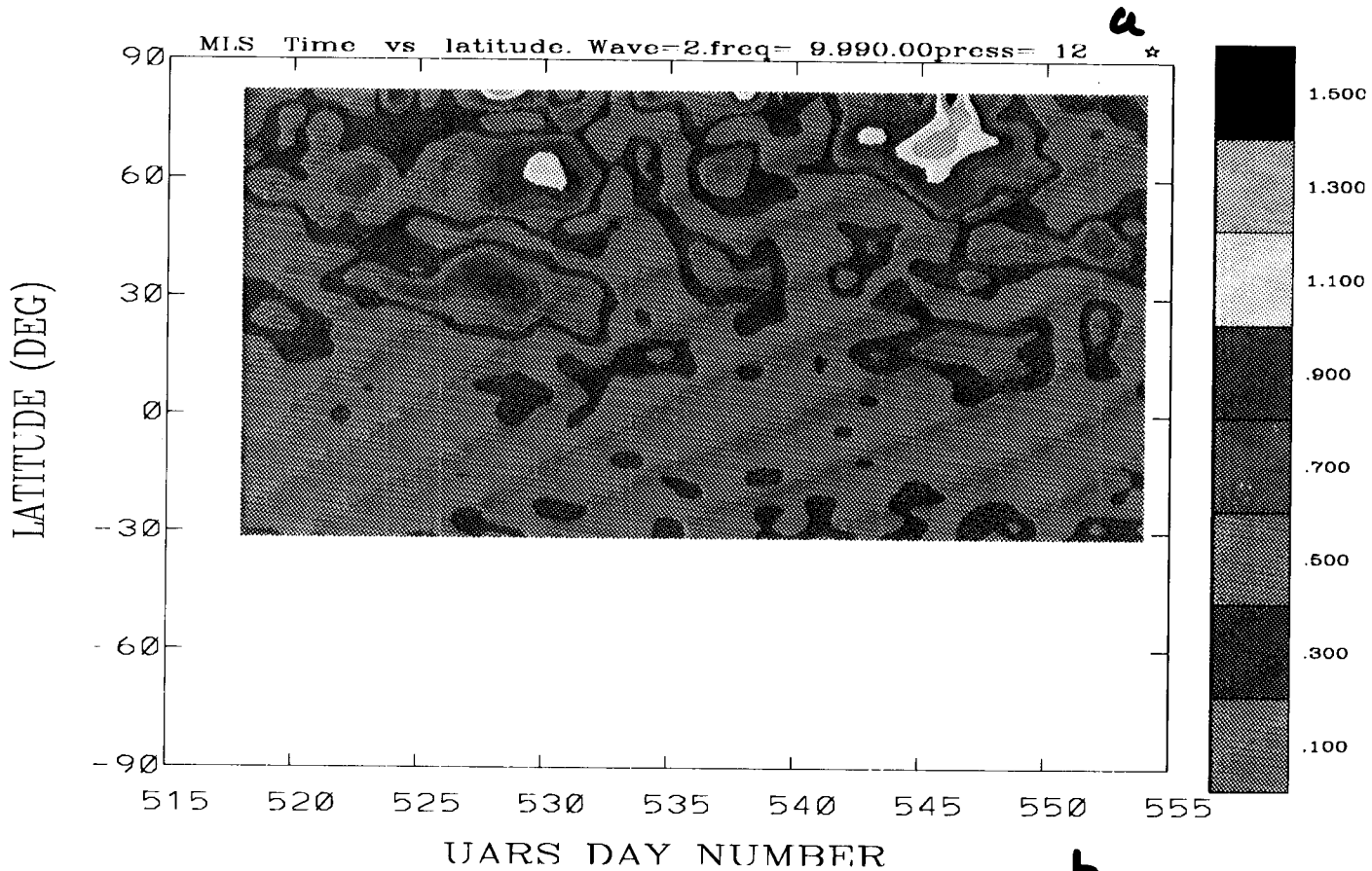
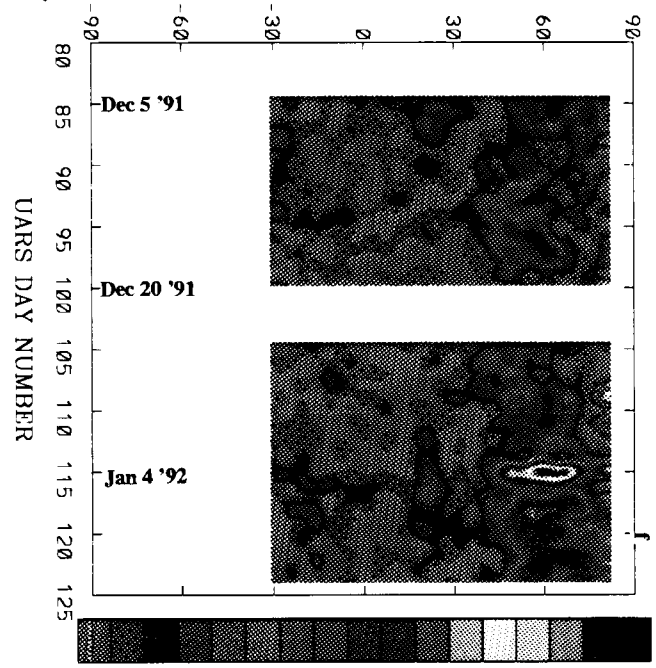
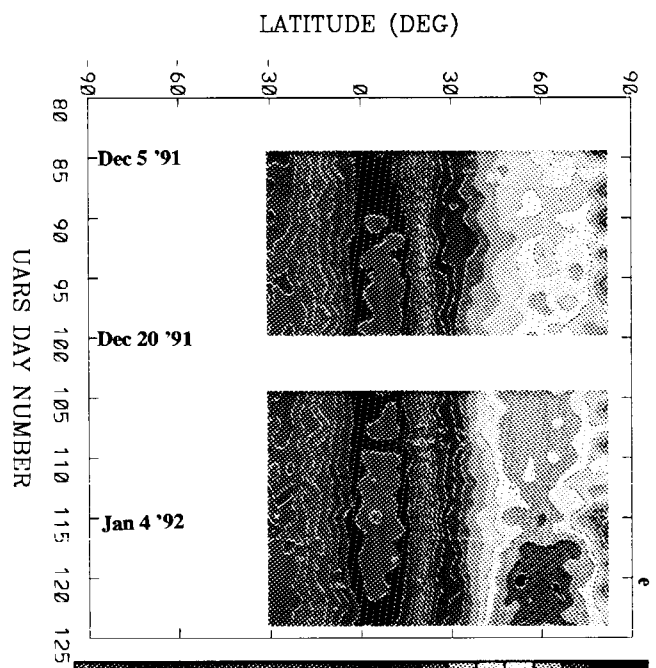
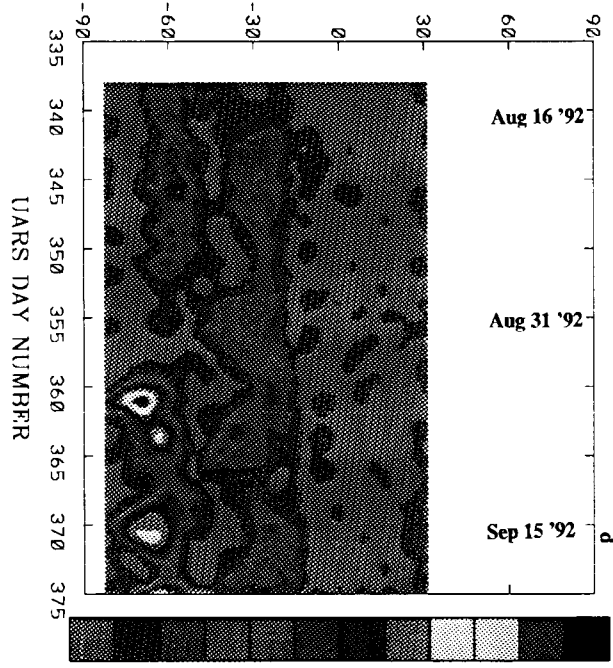
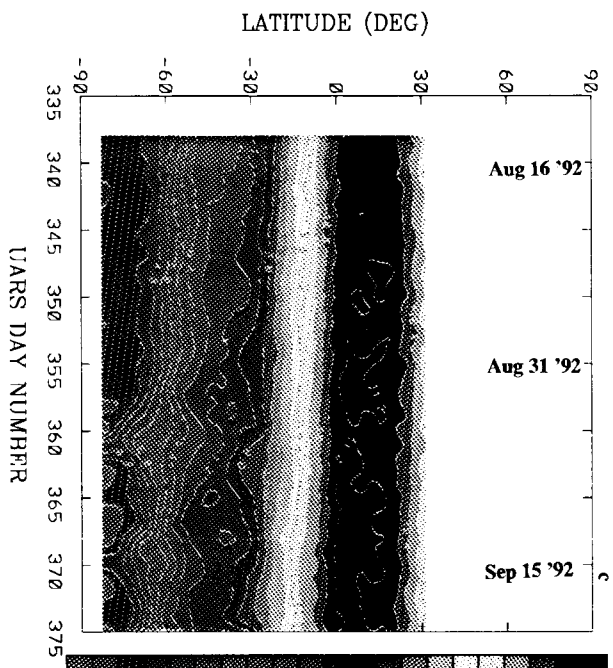
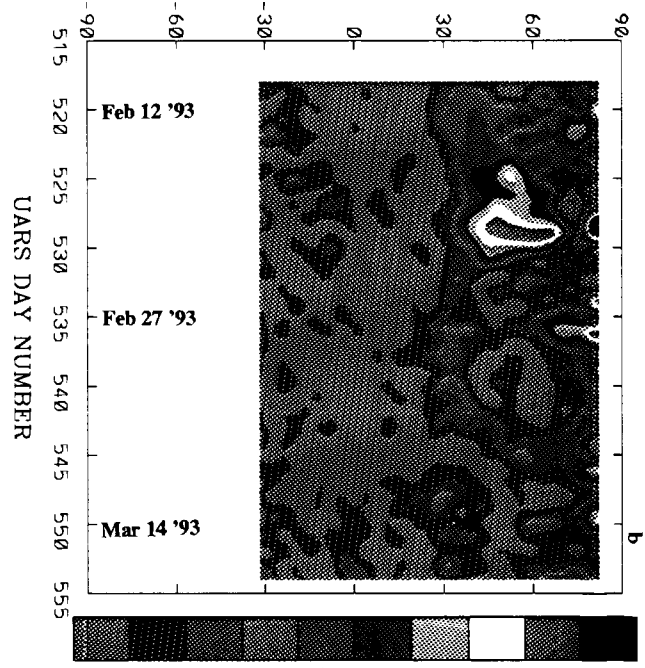
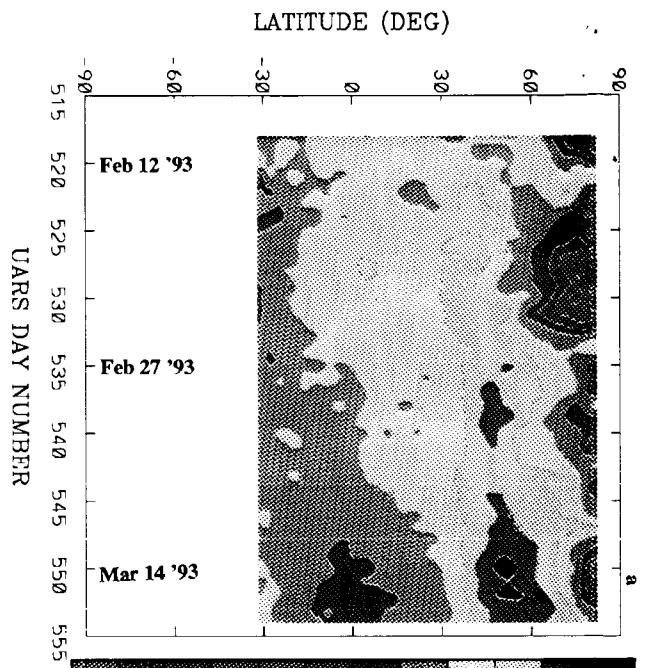


Fig 4



**Figs**

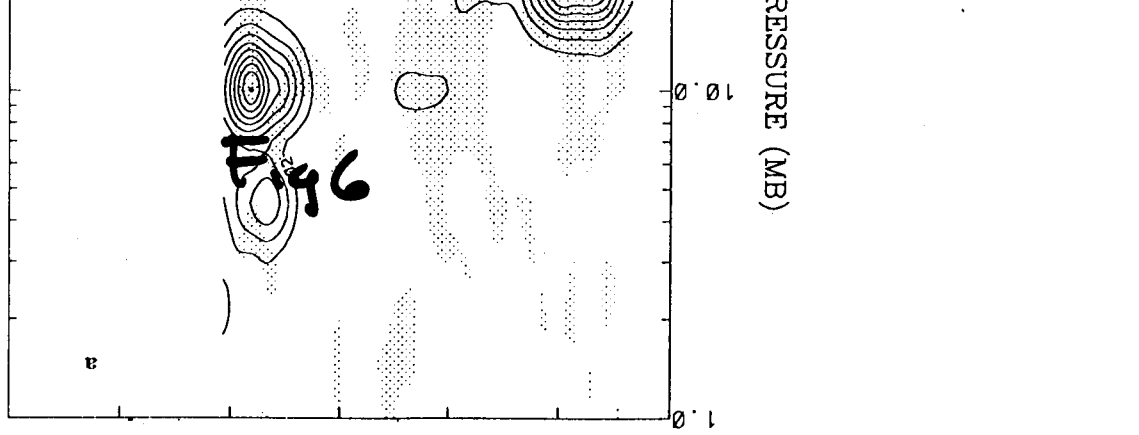
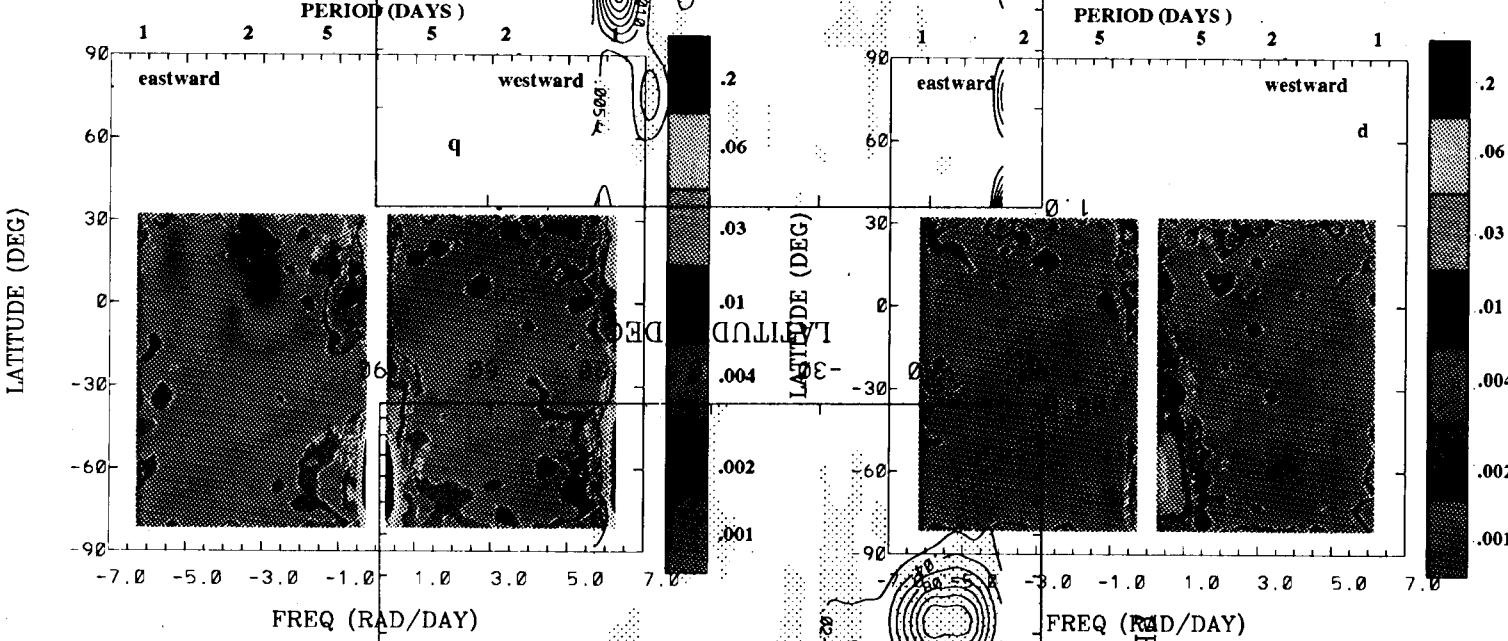
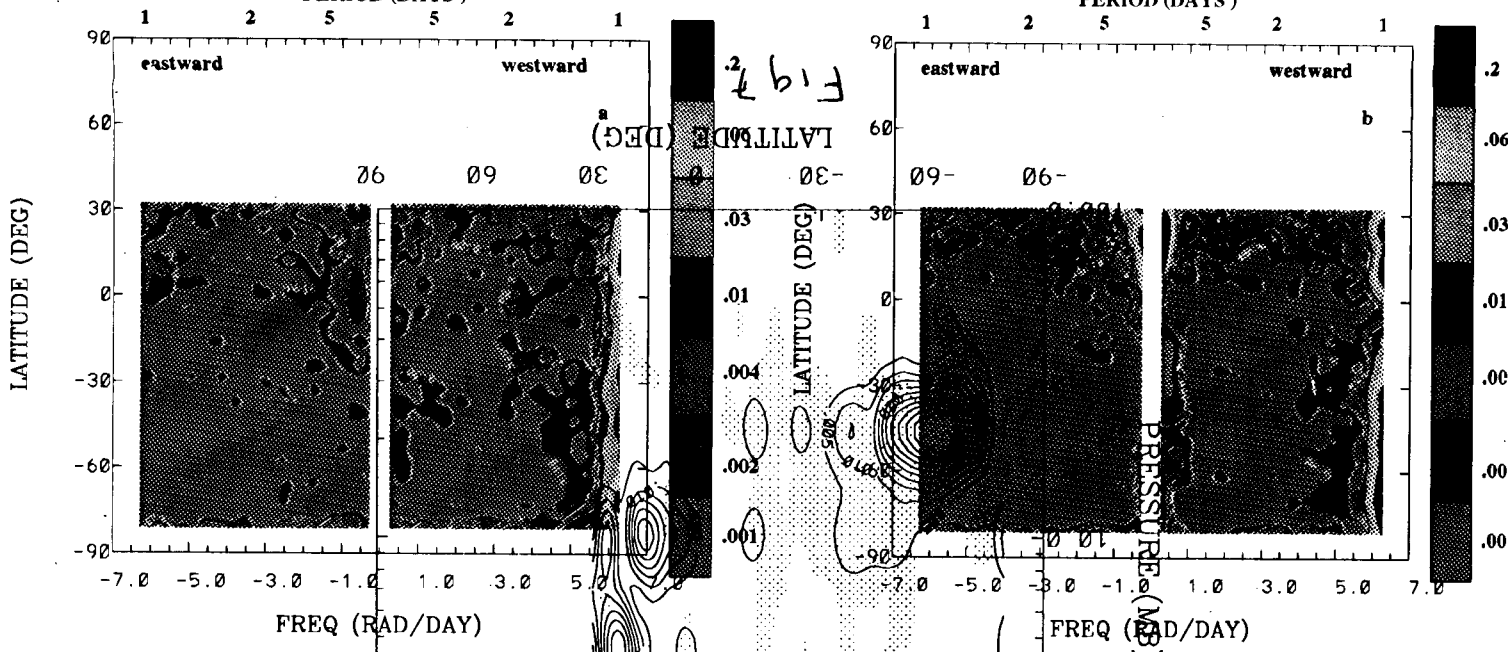


Fig 7

Fig 8

1

2

5

5

2

1

90

2

5

5

2

1

Fig 7

